Role of Surface Latent Heat Flux in Shallow Cloud Transitions: A Mechanism-Denial LES Study

YOUTONG ZHENG,[a] HAIPENG ZHANG,[a] AND ZHANQING LI[a]

[a] *Earth System Science Interdisciplinary Center, University of Maryland, College Park, College Park, Maryland*

ABSTRACT: Surface latent heat flux (LHF) has been considered as the determinant driver of the stratocumulus-to-cumulus transition (SCT). The distinct signature of the LHF in driving the SCT, however, has not been found in observations. This motivates us to ask, How determinant is the LHF to SCT? To answer this question, we conduct large-eddy simulations in a Lagrangian setup in which the sea surface temperature increases over time to mimic a low-level cold-air advection. To isolate the role of LHF, we conduct a mechanism-denial experiment in which the LHF adjustment is turned off. The simulations confirm the indispensable roles of LHF in sustaining (although not initiating) the boundary layer decoupling (first stage of SCT) and driving the cloud regime transition (second stage of SCT). However, using theoretical arguments and LES results, we show that decoupling can happen without the need for LHF to increase as long as the capping inversion is weak enough to ensure high entrainment efficiency. The high entrainment efficiency alone cannot sustain the decoupled state without the help of LHF adjustment, leading to the recoupling of the boundary layer that eventually becomes cloud-free. Interestingly, the stratocumulus sheet is sustained longer without LHF adjustment. The mechanisms underlying the findings are explained from the perspectives of cloud-layer budgets of energy (first stage) and liquid water path (second stage).

SIGNIFICANCE STATEMENT: An important but poorly understood phenomenon about the stratocumulus (low-lying blanket-like clouds) is its tendency to transition to cumulus clouds (cauliflower-like clouds) as the sea surface warms, called the stratocumulus-to-cumulus transition (SCT). We confirmed an existing hypothesis that an increase in the evaporation of seawater [latent heat flux (LHF)] is the key driver of the SCT. However, we found the role of LHF depends on environmental conditions. For example, if the temperature jump above the cloud is weak, the overlying warm air can sink more effectively into the cloud, initiating the boundary layer decoupling, the first phase of SCT. These results advance our understanding of the conditions under which SCT happens, allowing better quantification of its role in climate change.

KEYWORDS: Atmosphere; Conservation equations; Convective clouds; Large eddy simulations

1. Introduction

Marine stratocumulus (Sc) has the most extensive areal coverage among all cloud regimes (Hahn and Warren 2007). This, in combination with its net cooling effect (Hartmann et al. 1992), makes Sc one of the most important players in Earth's radiative budget (Wood 2012). An important phenomenon about the Sc is its tendency to transition to cumulus (Cu) clouds as it drifts over warm water (Riehl et al. 1951; Albrecht et al. 1995; Klein et al. 1995; Krueger et al. 1995; Bretherton 1997; de Roode and Duynkerke 1997; Zhou et al. 2015; Zheng et al. 2018). Such a cloud transition is well known to predominate over subtropical oceans, where equatorward trade winds generate cold-air advection, a necessary condition for the transition to happen. The Sc-to-Cu transition also occurs in the cold section of midlatitude cyclones (McCoy et al. 2017; Kazemirad and Miller 2020; Zheng et al. 2020) and polar

oceans during cold air outbreaks (Abel et al. 2017; Lloyd et al. 2018; Geerts 2019). Given the substantial impacts of the Sc-to-Cu transition on the regional and global radiative budgets and the difficulty of climate models in simulating it (Teixeira et al. 2011; Bodas-Salcedo et al. 2014; Neggers et al. 2017), it is imperative to continue making progress in understanding its underlying mechanism.

The Sc-to-Cu transition can be divided into two stages (Krueger et al. 1995; Wyant et al. 1997). Consider a radiatively driven well-mixed Sc-topped boundary layer (STBL). In the first stage, as the sea surface temperature (SST) increases, the STBL deepens over time. Accompanied with the deepening is the vertical stratification of STBL into two separate layers, with the upper Sc-containing layer being warmer and drier than the surface mixed layer, a phenomenon called decoupling (Nicholls 1984). After decoupling, Cu often develops on top of the surface mixed layer and detrains water into the Sc deck, forming a Cu-coupled STBL, a consequence of destabilization by cold-air advection. In the second stage, as the SST continues to increase, the convection shifts from radiatively driven to surface-flux driven, manifested as the dominance of cumuliform clouds and eventual dissipation of the stratiform clouds.

The increase in the latent heat flux (LHF) is widely considered the determinant driver of the transition. This view is based on, if not originates from, the theory of deepening–warming

Zheng's current affiliation: Atmospheric and Oceanic Sciences, Princeton University, and NOAA/Geophysical Fluid Dynamics Laboratory, Princeton, New Jersey.

Corresponding author: Youtong Zheng, zhengyoutong@gmail.com

decoupling developed by Bretherton and Wyant (1997, hereafter BW97). In the theory, LHF must increase due to the enhanced surface moisture gradient: the surface saturation moisture increases due to the Clausius–Clapeyron relationship, and the near-surface air moisture drops due to the entrainment of dry free-atmospheric air into the boundary layer. With stronger LHF, the buoyancy flux in the cloud layer will strengthen, invigorating cloud-scale turbulence that causes more entrainment warming per unit of cloud-top radiative cooling. This drives both stages of the cloud transition. In the first stage, the enhanced entrainment stabilizes the boundary layer. When the radiative cooling (that varies little relative to entrainment) is not strong enough to mix the entrained warm air throughout the boundary layer, decoupling happens (Lewellen and Lewellen 1998; Stevens 2000). In the second stage, the increased LHF invigorates Cu clouds that bump against the inversion, inducing bursts of increased entrainment of dry air into the cloud layer. This eventually dissipates the Sc sheets, leaving only Cu clouds (Wyant et al. 1997). This view of LHF as the driver of Sc-to-Cu transition is supported by a series of high-resolution modeling studies (Wyant et al. 1997; Sandu and Stevens 2011; Xiao et al. 2011).

Field observations, however, show different results. Jones et al. (2011) found that LHF cannot separate decoupled from well-mixed boundary layers using aircraft data collected over the subtropical southeast Pacific. Zhou et al. (2015), who used half-year observations collected from a cargo ship traveling between Los Angeles, California, and Honolulu, Hawaii, found a nearly unchanged LHF along the climatological transact of Sc-to-Cu transition. For this reason, Zhou et al. (2015) argued that the role of LHF in cloud transition is not as determinant as previously thought.

The lack of a clear signal of LHF impact on the transition in observations lends us to ask, How determinant the LHF is for driving the Sc-to-Cu transition? Some clues arise from BW97's own theory. In addition to LHF, other factors can also modify the coupling state of STBL such as the cloud-top radiative cooling, precipitation, and entrainment efficiency. On the time-scale characteristic of Sc-to-Cu transition, i.e., multiple days, the radiative cooling and precipitation do not change systematically (or by limited extent); thus, their roles are deemed by BW97 as less important. Different is the entrainment efficiency that, in BW97's simulation, systematically increases with the SST, promoting the decoupling in a similar way as the LHF does. The relative importance of the two factors is not thoroughly investigated.[1] One may argue that if the entrainment efficiency is sufficiently large, decoupling may happen regardless of changes in LHF. Indeed, Sandu and Stevens (2011) found that the cloud transition happens faster for an STBL capped by a weaker temperature inversion, a condition favorable for large entrainment efficiency (Nicholls and Turton 1986). As a result, to what degree the LHF controls the cloud transition should depend on other factors, in

particular, those controlling the entrainment efficiency (e.g., temperature and moisture jumps across the inversion).

This study aims to elucidate the roles of LHF in driving the Sc-to-Cu transitions using the large-eddy simulations (LESs). Unlike previous LES studies that evaluate the effect of LHF via indirect evidence (e.g., looking at moisture and buoyancy flux profiles), we isolate the role of LHF by turning off the LHF adjustment to the SST increase. Such a mechanism-denial experiment allows for a clearer interpretation of the impact of LHF.

The next section will introduce the models, the experiments, and methods for diagnosing key statistics. The main results are presented in section 3. Sections 4 and 5 are devoted to elucidating the underlying mechanisms of LHF influences on the STBL decoupling (first stage) and Sc dissipation (second stages) during the Sc-to-Cu transition, respectively. In section 4, we will interpret the STBL decoupling using the idea of cloud-layer energy balance developed by BW97. In section 5, dissipations of Sc decks in the control and mechanism-denial experiments will be discussed in the context of the theories of cloud-top evaporative instability (Deardorff 1980; Randall 1980) and the cumulus penetrative entrainment (Bretherton 1997; Wyant et al. 1997). We will quantify the controlling factors of Sc deck lifetime using the liquid water path (LWP) budget analysis (Van der Dussen et al. 2014). Sections 6 and 7 present the discussion and concluding remarks, respectively.

2. Models

We use both an LES model and a mixed-layer model (MLM) (Lilly 1968; BW97; Bretherton et al. 2010). An important merit of MLM is its analytic tractability, which offers a complementary view to interpret results from LES.

a. LES

We use the newest version of System for Atmospheric Modeling (SAM) model, version 6.11.6 (Khairoutdinov and Randall 2003). SAM is a nonhydrostatic anelastic model. The prognostic thermodynamic scalars are liquid water static energy, total nonprecipitating water mixing ratio, and total precipitating water mixing ratio. On a fully staggered Arakawa C–type grid, all the prognostic scalars are advected using a three-dimensional positive definite and monotonic scheme developed by Smolarkiewicz and Grabowski (1990). The second-order finite differences in the flux form with kinetic energy conservation are used for momentum. A variable step is adopted for time integration using the third-order Adams–Bashforth scheme. The subgrid-scale turbulence is handled by the 1.5-order subgrid-scale turbulent kinetic energy scheme. A simplified (drizzle only) version of Khairoutdinov and Kogan (2000) microphysics scheme is used for conversion between cloud and rainwater as well as raindrop evaporation and sedimentation. The drizzle number concentration is treated prognostically while the cloud droplet number concentration is prescribed as $100\,cm^{-3}$. The geometric standard deviation of the lognormal cloud droplet size distribution is set as 1.2. For the radiation scheme, we use the RRTMG (Iacono et al. 2008) that computes the radiative fluxes based on the correlated-k

---

[1] BW97 fixes the entrainment efficiency and found decoupling still occurs; however, this cannot demonstrate that LHF is the more dominant factor.

approach. The surface fluxes are computed from the Monin–Obukhov similarity theory.

This study is based on the simulation of Sc-to-Cu transition during the Atlantic Stratocumulus Transition Experiment (ASTEX) (Albrecht et al. 1995). As shown in Fig. 1a, the ASTEX case displays an evolution of STBL typical of Sc-to-Cu transition: boundary layer deepening, the emergence of sporadic Cu detraining into the Sc deck, and thinning of Sc deck as the Cu develops. During the ASTEX case, the SST increases by ~4 K over the 40-h simulation. Here we linearize the SST increase rate, yielding a Tadv = −2.6 K day^{-1} (Fig. 1c). Such a linearization of SST has the benefit of avoiding unnecessary complications due to a changing surface warming rate. Similarly, we use a diurnally averaged solar zenith angle of 68.72° to remove the influence of the diurnal cycle of solar insolation, because the cloud transition typically has a time scale of multiple days and the diurnal cycle only plays a minor role in the multiple-day transition. Other setups (e.g., initial sounding, mean subsidence, and geostrophic winds) are the same as those used in the ASTEX LES intercomparison project (Van der Dussen et al. 2013). Figure 1b shows the simulated evolution of STBL after the simplifications of surface and radiative forcing. The key features of the Sc-to-Cu transition holds well (Fig. 1a): the boundary layer deepening and decoupling, emergence of Cu, and breakup of the Sc deck.

In the control experiment (named "CTRL"), the LHF increases throughout the whole period of the simulation (solid line in Fig. 1c). We run the mechanism-denial experiment by fixing the LHF as the initial value of 67 W m^{-2}, called "FXDLHF."

The horizontal domain size is 4480 m × 4480 m with doubly periodic lateral boundaries. The horizontal resolution is 35 m and the vertical resolution varies from 15 m at the surface to 5 m in the cloud and the inversion layers. Above ~2400 m, the vertical grid size increases by 10% per level until the model top of ~4200 m. Increasing the horizontal domain size has a marginal influence on the simulations of weakly precipitating shallow clouds (Sandu and Stevens 2011), such as the case in our study. We confirm this idea by increasing our domain size to 8960 m × 8960 m and find that the results hold (see appendix).

1) DIAGNOSTIC STATISTICS

To measure the degree of boundary layer stratification, we adopt the method of Wyant et al. (1997) to average the liquid water potential temperature (θ_l) over the 75-m layers below the capping inversion and near the surface. Their difference
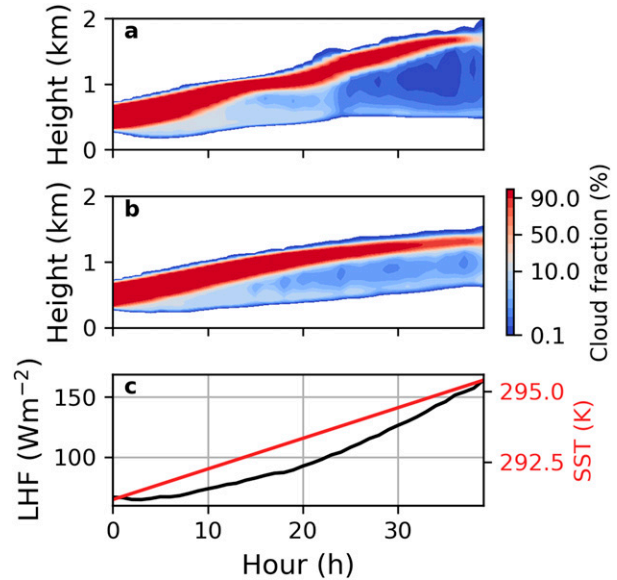

FIG. 1. Time–height profiles of SAM-simulated cloud fraction of ASTEX case with (a) original and (b) linearized forcing. (c) Temporal evolutions of latent heat fluxes and sea surface temperature (red) for the case in (b).

yields the thermal stratification of the STBL, namely, $\Delta_{\mathrm{BL}}\theta_l$. Similarly, we can diagnose the moisture stratification of $\Delta_{\mathrm{BL}}q_t$, in which the q_t is the sum of specific humidity of water vapor (q_v) and liquid water (q_l).

We determine the bottom and top of the capping inversion using the method of Yamaguchi and Randall (2008) that is based on the profile of θ_l variance. This enables quantification of the thermal and moisture jump across the inversion: $\Delta_{\mathrm{inv}}\theta_l$ and $\Delta_{\mathrm{inv}}q_t$. The cloud-base height of the Sc deck (z_b) is defined as the lowest altitude with cloudiness greater than 50%.

The entrainment rate w_e is diagnosed from the mass budget equation: $w_e = dz_i/dt - w_{\mathrm{sub}}$, in which z_i is the inversion-layer height and the w_{sub} is the subsidence rate at z_i. We compute the lifting condensation level (LCL) using the analytic formula developed by Romps (2017).

2) LWP BUDGET ANALYSIS

We use the budget analysis of LWP developed by Van der Dussen et al. (2013):

$$\frac{\partial \mathrm{LWP}}{\partial t} = \underbrace{\rho w_e \left(\eta \Delta q_t - \Pi \gamma \eta \Delta \theta_l - h_* \Gamma_{q_l} \right)}_{\text{Entrainment}} + \underbrace{\rho \eta [\overline{w'q_t'}(z_b) - \Pi \gamma \overline{w'\theta_v'}(z_b)]}_{\text{Cloud-base moisture flux}} + \underbrace{\rho \eta \gamma \Delta F_{\mathrm{rad}}}_{\text{Radiation}} + \underbrace{(-\rho \Delta P)}_{\text{Precipitation}} + \underbrace{(-\rho h_* \Gamma_{q_l} w_{\mathrm{sub}})}_{\text{Large-scale subsidenc}}, \quad (1)$$

in which ρ is the air density, Π is the Exner function, γ is the rate of change of saturation specific humidity with the absolute temperature (taken as 0.55 g kg^{-1} K^{-1}), h_* is the Sc thickness, Γ_{q_l} is the lapse rate of q_l, F_{rad} is the net radiative flux (K m s^{-1}), P is the precipitation flux (m s^{-1}), and $\overline{w'\theta_v'}(z_b)$ and $\overline{w'q_t'}(z_b)$ are eddy fluxes of θ_l and q_t at

cloud base, respectively. The η is a thermodynamic constant, computed as $[1 + (L_v\gamma)/c_p]^{-1}$, in which L_v is the latent heat of vaporization and the c_p is the specific heat of air at constant pressure. The Δ denotes the cloud-top value subtracted by cloud-base value. For ΔP, since precipitation flux is presumably zero at the top of the
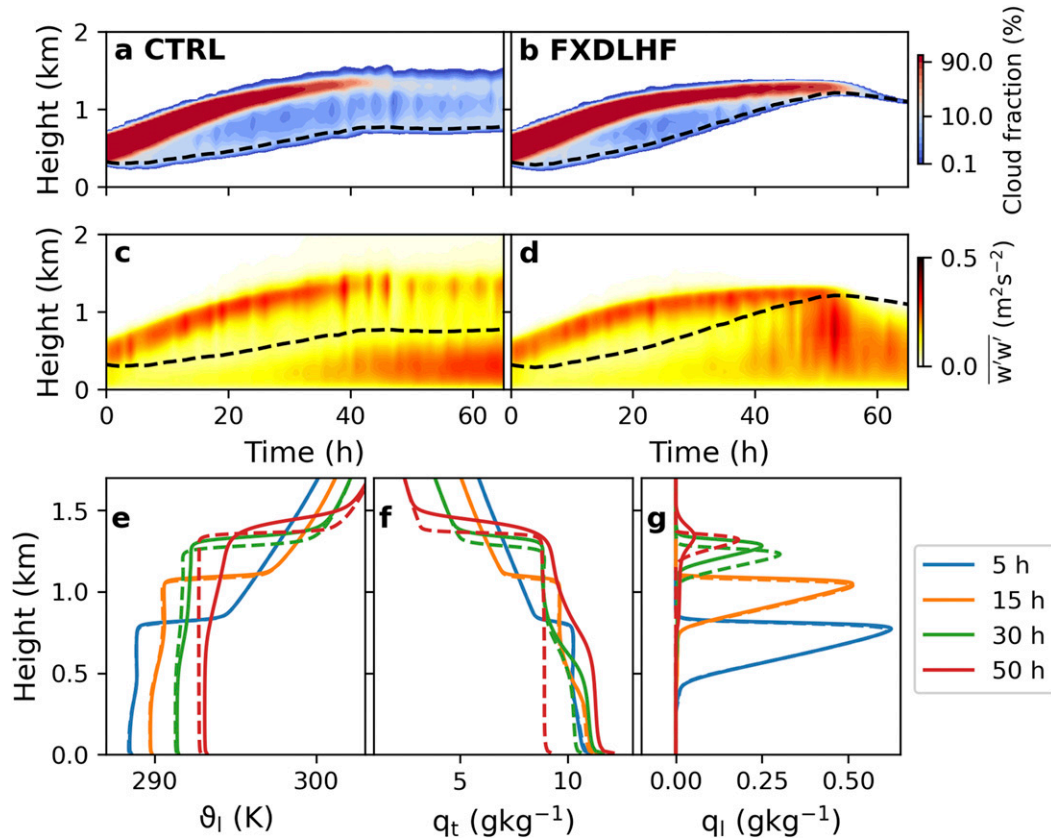
FIG. 2. Evolutions of STBLs in CTRL and FXDLHF runs. (a)–(d) The time–height plots of cloud fraction and vertical velocity variance for the (a),(c) CTRL and (b),(d) FXDLHF. The dashed line marks the lifting condensation level. (e)–(g) The vertical profiles of θ_l, q_t, and q_l, respectively, for CTRL (solid) and FXDLHF (dashed) at different times of the simulations.

cloud, the ΔP is nearly equivalent to the cloud-base precipitation flux. The five forcing terms on the right-hand side of the equation represent the contributions from the entrainment (Ent_{LWP}), turbulent fluxes at cloud base ($Base_{LWP}$), radiation (Rad_{LWP}), precipitation ($Prec_{LWP}$), and subsidence ($Subs_{LWP}$), respectively.

b. Mixed-layer model

The MLM we use is the same as that used in BW97. The model has three prognostic equations for the z_i, moist static energy, and q_t, which describes the budgets of mass, enthalpy, and moisture, respectively. Here we discuss two aspects of the MLM that are particularly relevant to this study.

First, the MLM diagnoses the decoupling based on the buoyancy integral ratio (BIR) defined as $BIR = -\int_0^{z_i} \overline{w'\theta_v'}\mathcal{H}(-\overline{w'\theta_v'})\,dz / \int_0^{z_i} \overline{w'\theta_v'}\mathcal{H}(\overline{w'\theta_v'})\,dz$, where $\mathcal{H}$ is the Heaviside function and θ_v is the virtual potential temperature. The physical meaning of BIR is the vertical integral of the negative buoyancy flux scaled by the vertical integral of the positive buoyancy flux. Following the BW97, we use a BIR threshold of 0.15, above which the STBL is considered decoupled and the MLM ceases to be valid.

Second, as will become obvious later, a variable central to the main argument of this study is the entrainment efficiency (denoted as A), a nondimensional parameter measuring the entrainment

rate for a given buoyancy inversion and turbulence level. The MLM parameterizes the A as (Nicholls and Turton 1986)

$$A = 0.2\left[1 + 60\left(1 - \frac{\Delta_m}{\Delta_{inv}s_v}\right)\right], \qquad (2)$$

where $\Delta_{inv}s_v$ is the difference in virtual static energy (s_v) across the inversion layer and Δ_m is twice the average of the difference between the s_v of entrained air across the inversion and the s_v of the saturated air at the cloud top. As elaborated in Nicholls and Turton (1986), A is a measure of the strength of evaporative cooling. Physically speaking, a weaker buoyancy inversion, drier free atmosphere, and juicier clouds favor the evaporation of cloud water, although the quantitative detail of their combined control is complex. Note that Eq. (2) is an idealized approximation of A. Strictly speaking, it does not explicitly include some factors such as the radiative cooling (Stevens 2002), cloud droplet sedimentation (Bretherton et al. 2007), and other less known A-controlling factors such as the turbulence regime (Wyant et al. 1997).

3. Results on the back of the envelope

Figure 2 shows the evolutions of STBL in the CTRL and FXDLHF simulations from which we may infer the influences of LHF as follows.

In the first stage of boundary layer decoupling (the first tens of hours), LHF appears to play no role in the initial decoupling. As shown by the sounding (Figs. 2e,f), both simulations show boundary layers stratifying over the first 15 h. This trend can be quantified by the evolutions of $\Delta_{BL}\theta_l$ and $\Delta_{BL}q_t$ (Fig. 3) showing an increasing degree of decoupling during $t = 0$–15 h for both runs. From $t = 15$ h onward, the $\Delta_{BL}\theta_l$ (or the $\Delta_{BL}q_t$) starts to diverge between the two runs. In the FXDLHF, the boundary layer recouples, as seen from the decreased stratification (Fig. 3) and the reduced distance between the base of the Sc deck and LCL (Fig. 2c). The results suggest that fixing the LHF does not prevent the boundary layer from decoupling, but the decoupled state cannot be sustained.

In the second stage of Sc dissipation, fixing the LHF eventually results in a cloud-free boundary layer without any Cu clouds left. Sc decks dissipate in both simulations but in different ways. In the CTRL, the Sc deck breaks up as the cumulus clouds shooting into the Sc deck (Fig. 2a), a regime characteristic of the typical Sc-to-Cu transition. In the FXDLHF, however, the Sc sheet dissipates in a well-mixed STBL in which the drying of the boundary layer (Fig. 2f) elevates the LCL. The LCL gradually approaches the boundary layer top, thinning the Sc deck over time (Fig. 2c). This eventually leads to a clear boundary layer. Such a difference of the Sc dissipation between the two runs can also be seen from the dynamic fields (e.g., vertical velocity variance shown in Figs. 2b,d). In the CTRL, the vertical velocity variance has two separate peaks during the breakup, one below the inversion and one in the subcloud layer, which is a manifestation of the Cu-fed Sc regime. In the FXDLHF, the vertical velocity variance profile tends toward a single peak from $t = 50$ h onward when the cloud dissipates, a manifestation of a well-mixed STBL. Interestingly, the Sc deck is sustained longer in FXDLHF than the CTRL run (Fig. 3c).

In a summary, decoupling happens in both runs, but the decoupled state cannot be sustained in the FXDLHF in which the decoupled boundary layer eventually recouples. In the FXDLHF, the lack of moisture supply from the surface dries the boundary layer over time, which eventually dissipates the Sc deck, leading to a clear boundary layer. Therefore, the transition to Cu regime does not happen without an increase in LHF. Despite the lack of moisture supply in FXDLHF, Sc deck is sustained for ~10 h longer than that in CTRL.

A series of questions arise: Why does decoupling still happen even if the LHF is not allowed to increase? Why does the boundary layer recouple after initial decoupling in the FXDLHF? Can the FXDLHF results be explained by the theoretical framework of BW97? Why is the Sc sustained longer in the FXDLHF even though the surface moisture supply is weaker? How can the Sc dissipations in both runs be explained with existing theories such as the cloud-top entrainment instability (Randall 1980; Deardorff 1980) and "cumulus penetrative entrainment" theory (Wyant et al. 1997)?

To answer these questions, we will delve into the underlying mechanisms of the STBL decoupling and cloud dissipation in sections 4 and 5, respectively. Readers who are eager to find quick answers can find them in the last paragraph of section 5.
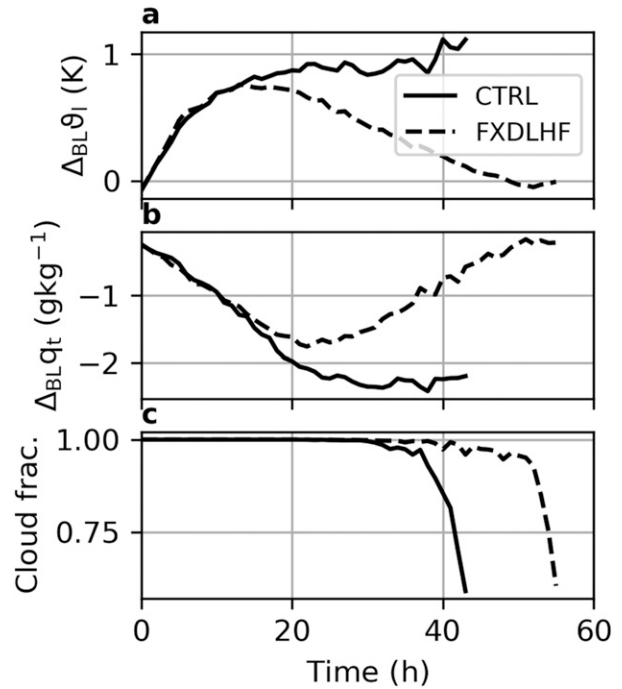

FIG. 3. Temporal evolutions of the boundary layer (a) thermal and (b) moisture stratifications and (c) cloud fraction.

4. First stage: STBL decoupling

a. A theoretical inquiry

We use the cloud-layer energy balance to guide our investigation, inspired by BW97. We begin by considering a variable that measures the buoyancy for cloudy air, namely, the virtual liquid water potential temperature:

$$\theta_{vl} = \theta_l + (0.61\theta_{ref})q_t, \tag{3}$$

in which θ_{ref} is a reference potential temperature, taken as a fixed value (290 K) representative for the cloud layer. θ_{vl} is physically similar to the density potential temperature in Emanuel (1994) and Stevens (2007) and the liquid water virtual static energy in BW97.

There are two benefits of using θ_{vl}. First, it is a linear combination of two adiabatically conserved variables (i.e., θ_l and q_t), which renders its analytical treatment easier. Second, in unsaturated flow, the $\theta_{vl} = \theta_v$. This bridges the θ_{vl} budget in the cloud layer to the subcloud buoyancy flux through the $\overline{w'\theta'_{vl}} = \overline{w'\theta'_v}$ at $z = z_b$. As will be elaborated later, this association is crucially important for understanding the STBL decoupling.

To derive a budget equation for θ_{vl} in the cloud layer, we start with the budget equations for θ_l and q_t:

$$h\frac{\partial \theta_l}{\partial t} = w_e \Delta_{inv}\theta_l - \frac{1}{\prod}\left(\Delta F_{rad} - \frac{L_v}{c_p}\Delta P\right) + \overline{w'\theta'_l}(z_b), \tag{4a}$$

$$h\frac{\partial q_t}{\partial t} = w_e \Delta_{inv}q_t - \Delta P + \overline{w'q'_t}(z_b). \tag{4b}$$

Combining (4a) and $0.61\theta_{\text{ref}} \times$ (4b) yields

$$h\underbrace{\frac{\partial\theta_{vl}}{\partial t}}_{\text{Stor}} = \underbrace{w_e\Delta_{\text{inv}}\theta_{vl}}_{\text{Ent}} - \underbrace{\frac{\Delta F_{\text{rad}}}{\Pi}}_{\text{Rad}} + \underbrace{\left(\frac{L_v}{c_p\Pi} - \mu\right)\Delta P}_{\text{Prec}} + \underbrace{\overline{w'\theta_{vl}'}(z_b)}_{\text{Base}},$$

(5)

in which h is the boundary layer depth and $\mu = 0.61\theta_{\text{ref}}$. The budget terms from the left to the right are storage term (Stor), entrainment warming (Ent), diabatic cooling by radiation (Rad), diabatic heating by precipitation (Prec), and θ_{vl} flux through the cloud base (Base). Rad + Prec yields the diabatic cooling term, denoted as Diab.

The budget formula can help us understand the STBL decoupling. A key signature of STBL decoupling is the emergence of negative buoyancy fluxes below the cloud base (Bretherton 1997; Stevens 2000). The more intense the negative buoyancy flux is, the more likely the STBL is decoupled. At the cloud base, the buoyancy flux $\overline{w'\theta_v'} = \overline{w'\theta_{vl}'}$ which is the Base term in Eq. (5). Thereby, STBL decoupling can be understood as the Base term smaller than a negative critical value. Assuming the Stor term remains considerably smaller than the forcing terms, the following processes, via favoring a decrease in Base, promote the decoupling:

- An increase in the entrainment
- A decrease in the cloud-top radiative cooling
- An increase in the precipitation

The three decoupling-promoting processes are consistent with our previous knowledge (Nicholls 1984; Nicholls and Leighton 1986; Bretherton 1997; Wood 2012). This framework can help us conceptualize how LHF is associated with the STBL decoupling. An increase in LHF will strengthen the buoyancy in the cloud layer through latent heating, increasing the $\overline{w'\theta_v'}$ averaged over the boundary layer, denoted as $\overline{w'\theta_v'}$. The increased $\overline{w'\theta_v'}$ will increase the Ent according to the entrainment closure of Turton and Nicholls (1987):

$$w_e\Delta_{\text{inv}}\theta_v = A\overline{\overline{w'\theta_v'}}.$$

(6)

Therefore, an increase in LHF promotes decoupling. This is the key idea of BW97's deepening–warming theory.

The above discussion offers several important insights into the relationship between the LHF and decoupling. First, it is the absolute value of LHF, not its temporal evolution, that directly determines the STBL decoupling. Imagine an STBL starting with an LHF large enough to cause excessive entrainment warming than the diabatic cooling, the STBL will decouple even if the LHF remains unchanged. In that regard, observations of unchanged LHF along the Sc-to-Cu transitions cannot disapprove of the deepening–warming theory (e.g., Zhou et al. 2015). Second, in addition to the LHF, the entrainment efficiency A is equally important in determining the decoupling. According to Eq. (6), an increase in A can yield the same results as the enhanced LHF does. Past works suggest that the A should increase with the cloud-top evaporative cooling (Nicholls and Turton 1986) and radiative cooling, with both dependent upon the properties of the cloud layer (e.g.,
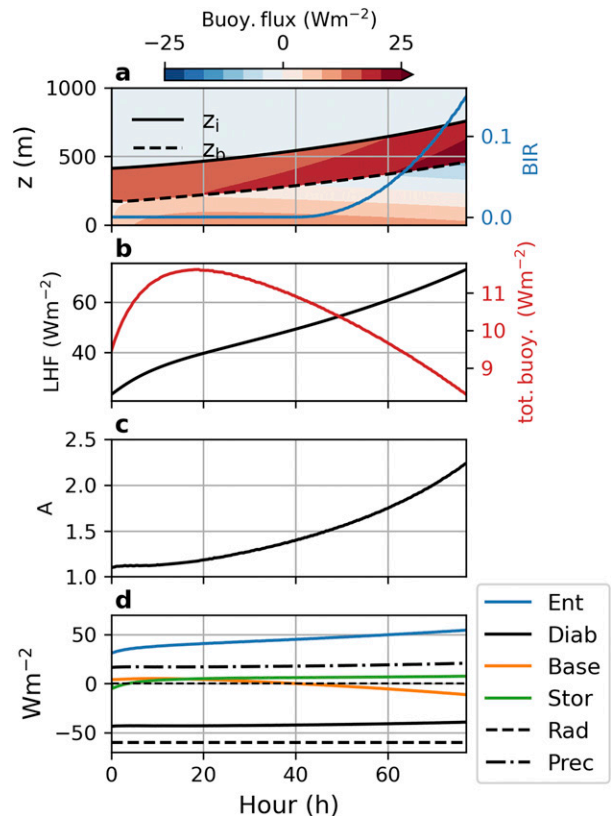

FIG. 4. MLM simulation of the control case. (a) A time–height plot of buoyancy flux and time evolutions of cloud boundaries and BIR. Temporal evolutions of (b) LHF and STBL-averaged buoyancy flux, (c) entrainment efficiency, and (d) cloud-layer energy budgets.

liquid water content) and inversion layer (e.g., thermodynamic properties of the overlying air). There is also evidence suggesting that the regime of boundary layer turbulence (e.g., cumulus-like versus stratocumulus-like) can modify the A (Wyant et al. 1997).

b. MLM simulation

To elucidate the role of LHF, we run the MLM to examine how the budget terms in Eq. (5) evolve during the transition. We specify the radiative cooling as $60\,\text{W}\,\text{m}^{-2}$ throughout the simulations to simplify the analysis, allowing us to focus on the role of LHF. This simplification should be tenable given that time variations of the radiative cooling, either in diurnal or multiple-day time scales, have marginal influences on the systematic cloud transitions (Bretherton 1997; BW97).

We first run a control case in an environment typical of the subtropical eastern Pacific. The case setup is the same as BW97 (see their Table 1 for simulation parameters). To summarize briefly, the initial SST is 285 K that increases by $1.5\,\text{K}\,\text{day}^{-1}$. The initial capping inversions of temperature and moisture are 13.2 K and $-4.2\,\text{g}\,\text{kg}^{-1}$, respectively. The large-scale divergence, horizontal wind, and free tropospheric moisture are held constant throughout the simulation. Figure 4a shows the evolution of the boundary layer of the control case. The STBL deepens
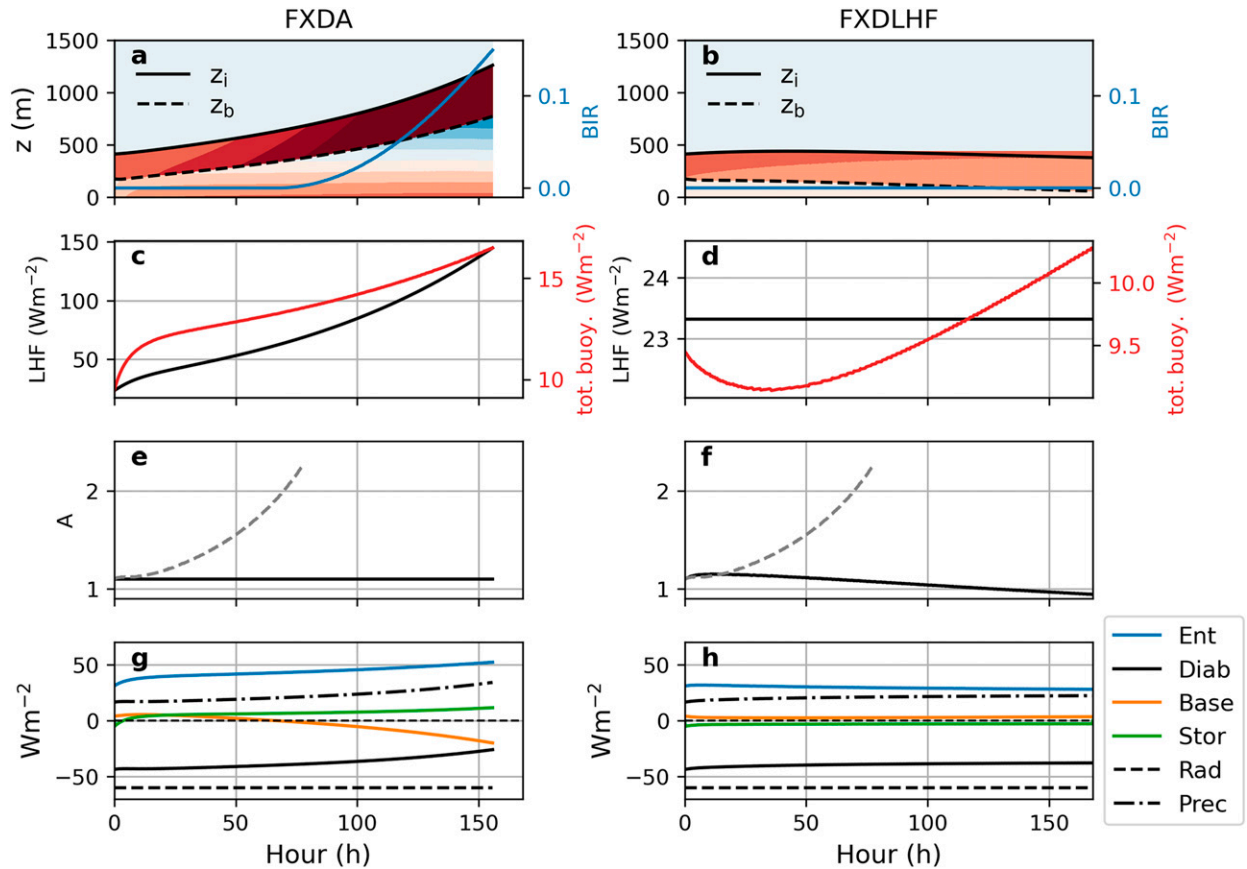
FIG. 5. As in Fig. 4, but for (left) FXDA and (right) FXDLHF cases. (e),(f) The time variation of A in the control case (dashed line) is plotted as a reference.

over time, accompanied by increasingly negative buoyancy flux below the cloud base, which eventually causes decoupling.

Such a decoupling process can be understood from the perspective of the cloud-layer energy budget (Fig. 4d). The Ent increases throughout the simulation, whereas the Diab changes very little. Such excessive warming has two consequences. First, the cloud layer heats up (i.e., Stor increases). Second, to balance the excessive warming, the buoyancy flux near the cloud base must shift from positive to negative (i.e., Base decreases), eventually causing decoupling.

Increases in LHF and A jointly contribute to the decoupling. The role of LHF is clearly seen on the first day when the LHF increases rapidly, raising the turbulent kinetic energy (TKE) production (Fig. 4b). The stronger turbulence is responsible for the initial increase in the Ent, an expected consequence of Turton and Nicholl's (1987) entrainment closure. From the first day onward, as the STBL deepens and erodes into the dry free atmosphere, A increases due to enhanced evaporative cooling (Fig. 4c), further strengthening the Ent. Such strengthened entrainment tends to suppress the boundary layer turbulence even though the LHF keeps increasing. Overall, increases in LHF and A jointly enhance the Ent that drives the decoupling.

To examine the individual roles of LHF and A, we run two simulations by fixing A and LHF as their respective initial

values (Fig. 5), noted as "FXDA" and "FXDLHF," respectively. In FXDA, the boundary layer still decouples but at a much slower rate than the control case. Without the adjustment in A, an increase in LHF strengthens the boundary layer turbulence and deepens the cloud depth via more latent heating and moisture supply, respectively. These two effects cause enhanced Ent and Prec, both promoting decoupling. However, the increasing rate of Ent is considerably slower than the control case due to the fixed A (Fig. 5). This, again, supports the importance of A feedback in decoupling.

In the FXDLHF run, the STBL remains coupled throughout the simulation. Without the increase in LHF, Ent remains noticeably smaller than the Diab. To balance the excessive cooling, the system must maintain a positive Base, which sustains the well-mixed STBL. More importantly, the relatively weak entrainment prevents the boundary layer from deepening so that the property of the capping inversion varies little, leading to a little varied A. Actually, A decreases slightly due to the shallowing of the boundary layer. This helps maintain the coupling state.

In addition to confirming BW97's idea that increasing the LHF alone is enough to drive decoupling, the above analysis stresses the significant role of the feedback associated with A. Compared with the control case, the A in both simulations are
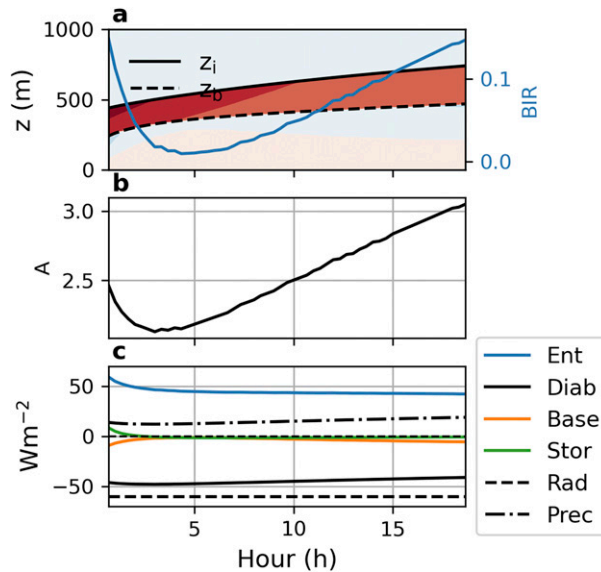
FIG. 6. As in Fig. 4, but with fixed LHF and halved initial temperature jump across the capping inversion.

FIG. 7. The capability of Ent + Diab in dictating decoupling. Temporal evolutions of Ent + Diab (solid) and BIR (dashed).

considerably smaller, leading to either much slower decoupling (FXDA) or no decoupling at all (FXDLHF), depending on the LHF. Such an important role of A may help us explain why the boundary layer decouples in the first 15 h of the LES FXDLHF experiment (Fig. 3). Unlike the MLM case that is capped by a strong inversion with a temperature jump of 13.2 K, the LES case (i.e., ASTEX) has a $\Delta_{inv}\theta_l$ of only 5.5 K. Everything else being equal, a weaker inversion typically corresponds to a larger A (Nicholls and Leighton 1986), promoting the decoupling. To test this hypothesis of A-induced decoupling, we repeat the MLM FXDLHF experiment, but initialize the case with a weaker temperature inversion (half as much). As shown in Fig. 6, the STBL decouples after ~20 h. Although the increase in Prec term contributes considerably to the eventual decoupling, the weak inversion maintains a large A, which sustains a large Ent throughout the simulation, allowing the decoupling to happen. This result is consistent with the finding from Sandu and Stevens (2011) that the Sc-to-Cu transition happens faster if the capping inversion is weaker.

In a summary, we learn two lessons from the MLM simulations. First, for a given diabatic cooling, decoupling is jointly controlled by the surface forcing (via the LHF) and the overlying atmospheric stability and humidity (via the A). Second, the relative magnitude of Ent and Diab is a diagnostic variable useful for understanding the decoupling. This can be more clearly illustrated in Fig. 7 showing the evolutions of Ent + Diab and BIR for the four MLM simulations: CTRL, CTRL FXDA, CTRL FXDLHF, and WEAK INV FXDLHF. STBLs with larger Ent + Diab are more likely to decouple and decouple at faster rates. This makes the Ent + Diab a useful parameter to interpret LES results. A long-lasting challenge of interpreting LES-simulated decoupling is that the geometry of the buoyancy flux profile is more complicated in LES than in MLM. As argued by Lewellen and Lewellen (1998), an
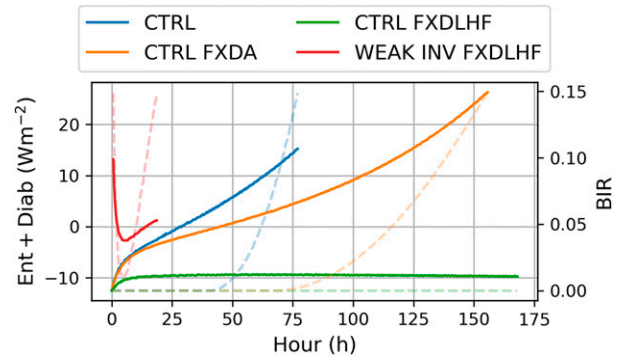
increase in entrainment tends to weaken the STBL-integrated buoyancy not only by increasing negative buoyancy fluxes in the subcloud layer but also by modifying the entire buoyancy geometry in a way that remains poorly understood. For example, if the radiative cooling concentrates at a thinner-than-usual layer, the entrained warm air may be cooled to the extent that negative buoyancy flux does not occur at any level even though the energetic cost of the entrainment still exists, manifested by lessened positive buoyancy flux. Moreover, under the condition of cold advection, the occurrence of cumulus-coupled STBL further complicates the geometry of the buoyancy flux profile (Bretherton and Blossey 2014). These issues could be circumvented by using Ent + Diab as a physically robust diagnostic to interpret decoupling.

c. LES

After the theoretical and MLM inquiries, we return to interpreting the LES simulations. In particular, we will utilize the Ent + Diab to interpret the time evolutions of decoupling. Figure 8a shows the Ent + Diab for the LES CTRL (solid red) and FXDLHF runs (dashed red). The Ent + Diab is markedly positive in the beginning 15 h for both simulations. Such sizable excessive heating explains the STBL decoupling (Figs. 8e,f). Although the radiative cooling increases[2] by ~10 W m^{-2} during the period of the first 15 h (Fig. 8b), the entrainment heating increases (Fig. 8c) by a larger extent (~25 W m^{-2}), so that the Ent + Rad overall increases. The Prec initially increases but decreases after $t = 6$ h, which is responsible for the inverted-U shape of the Ent + Diab, but does not alter the overall increasing trend of the Ent + Diab during $t = 0$–15 h. From $t = 15$ h onward, the two curves of Ent + Diab diverges. In FXDLHF, the decreasing trend of Ent + Diab well explains the recoupling of the boundary layer after $t = 15$ h (Fig. 8e). In CTRL, the Ent + Diab remains large, explaining the sustained decoupling.

Such a divergence of Ent + Diab between the two experiments reflects the role of LHF. In the CTRL, the increasing

---

[2] The radiative cooling strengthens primarily because of the intrusion of the boundary layer into drier free atmosphere, leading to lessened downward thermal flux at the cloud top.
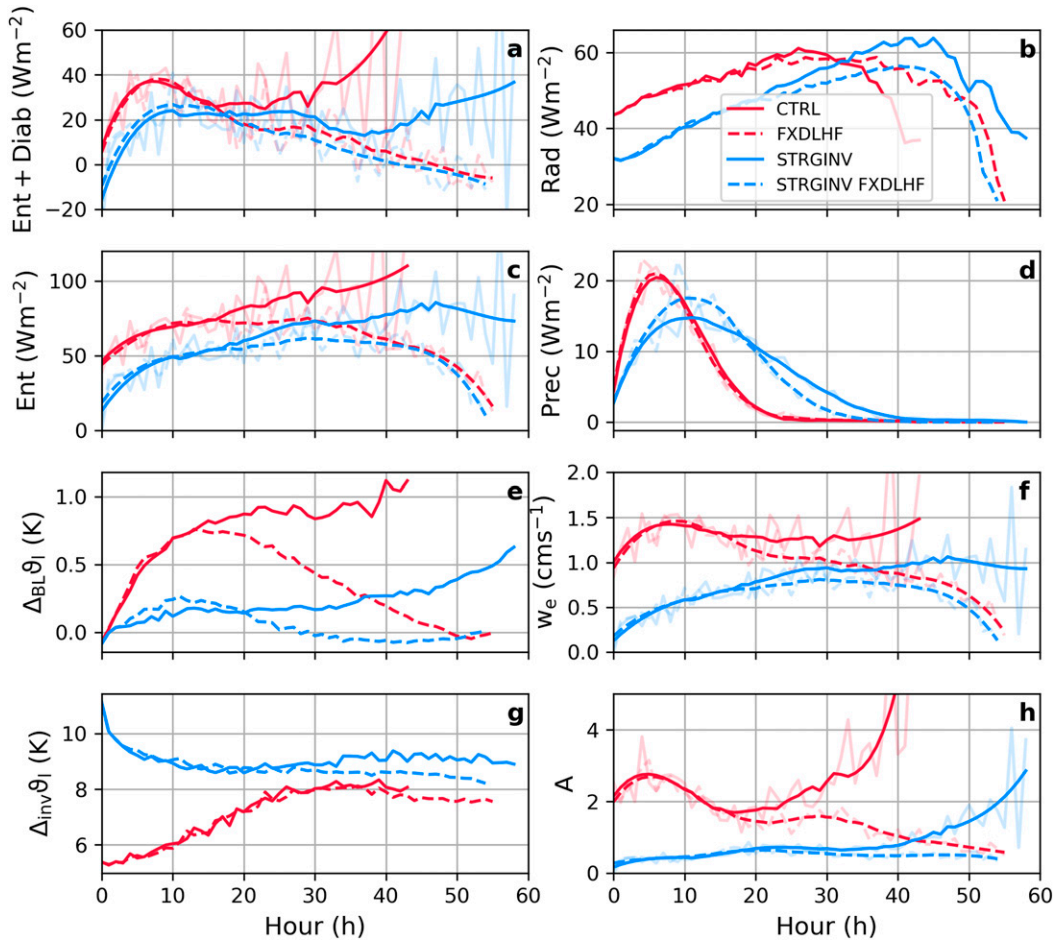
FIG. 8. Temporal evolutions of key LES diagnostics for the four LES experiments: CTRL (red solid), FXDLHF (red dashed), STRGINV (blue solid), and STRGINV FXDLHF (blue dashed). Variables diagnosed from w_e are smoothed to more clearly reflect the trend (intermittent cumulus convection causes large variances in these quantities). The unsmoothed values are marked by the semitransparent lines.

LHF generates sufficient in-cloud buoyancy to sustain w_e (Fig. 8f) so that the Ent remains large enough to overcome the diabatic cooling, thereby maintaining the decoupled state (Fig. 8a). Such large entrainment also dries the cloud liquid water more effectively, eventually reducing the Rad (Fig. 8b), which constitutes positive feedback that breaks up the stratocumulus decks. In the FXDLHF run, without an increase in LHF, the large entrainment rate is difficult to be sustained (Fig. 8f), primarily because of the strengthened temperature jump across the inversion (Fig. 8g). Moreover, the precipitation decreases (Fig. 8d) and radiative cooling strengthens (Fig. 8b), both contributing to stronger diabatic cooling and thus promoting recoupling.

In a summary, the evolution of the STBL coupling state can be well explained by the Ent + Diab. By fixing LHF, decoupling can still occur because the initial Ent + Diab is large enough to promote the decoupling. Such decoupling can only be sustained for 15 h, after which the boundary layer recouples primarily due to the LHF not sufficiently large to sustain the entrainment.

What causes such a large Ent + Diab at the beginning? As discussed in the MLM simulations, a large Ent can be attributed to a large A that is sensitive to the mixing properties between the Sc deck and the overlying air of the capping inversion. The ASTEX case has a $\Delta_{inv}\theta_l$ of only 5.5 K, which is smaller than typical extensive Sc decks over the eastern subtropics (Wood and Bretherton 2006). This favors more efficient entrainment and, thus, large Ent + Diab. To test the hypothesis, we repeat the two LES experiments by doubling the $\Delta_{inv}\theta_l$ of the initial sounding. The two new experiments are named "STRGINV" and "STRGINV FXDLHF," respectively. To infer the A from the LES data, we use Eq. (6). We replace the vertically averaged buoyancy flux with the turbulent dissipation averaged over the 200 m below the capping inversion because the latter is suggested to better represent the turbulence effect on entrainment (Bretherton and Blossey 2014).

The two new runs with stronger inversion are marked by the blue lines in Fig. 8. Indeed, the A is substantially smaller when the inversion strength doubles (Fig. 8h). The smaller A leads to smaller Ent (Fig. 8c) and thus smaller Ent + Diab (Fig. 8a),
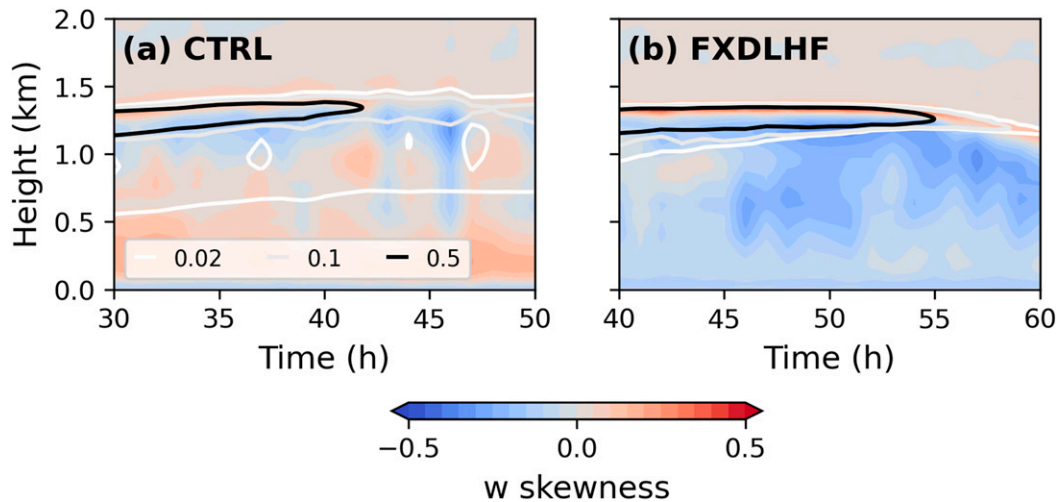
FIG. 9. Time–height plots of the vertical velocity skewness during the breakup stage for CTRL (30–50 h) and FXDLHF (40–60 h). The lines mark the cloud cover (unitless).

resulting in more coupled STBLs (Figs. 8e,f). This confirms our hypothesis. Comparing the STRGINV and STRGINV FXDLHF leads to similar conclusions on the role of LHF in decoupling that has already been discussed.

5. Second stage: Dissipation of stratocumulus deck

Fixing the LHF delays the breakup of the stratocumulus sheet by ~10 h (Fig. 3c). This section aims to figure out what causes the late dissipation.

There are two potential mechanisms for the dissipation. The first is the theory of cloud-top entrainment instability (CTEI) (Lilly 1968; Deardorff 1980; Randall 1980). This mechanism is based on the idea that the warm and dry air entrained across the inversion can mix with the saturated air. The evaporative cooling of the mixture can, in certain conditions, lead to negatively buoyant downdrafts, which enhances the entrainment by generating the TKE, forming a positive effect. Such a runaway effect dissipates the clouds. This mechanism is expressed in terms of a parameter $\kappa = 1 + (c_p/L_v)(\Delta\theta_l/\Delta q_t)$. The runaway effect can occur if the κ is greater than a critical value although the exact threshold remains uncertain (Kuo and Schubert 1988; Siems et al. 1990; Siems and Bretherton 1992; Stevens et al. 2003; Yamaguchi and Randall 2008; Lock 2009; Van der Dussen et al. 2014).

The second mechanism is proposed by Wyant et al. (1997), who argue that the breakup of Sc deck is caused by the Cu penetrative entrainment (CuPE). They found that in the Cu-fed Sc regime the Cu convection can both desiccate and moisten the Sc by promoting entrainment drying and by enhancing upward fluxes of moisture, respectively. The ratio between the two, defined as the "cumulus entrainment efficiency," gradually increases as the STBL deepens, which acts to dissipate the Sc deck.

The two mechanisms focus on different aspects of Sc dissipation. The CTEI stresses the significance of jumps of moisture and temperature above the Sc deck whereas the CuPE centers

on the preexisting turbulence in the boundary layer. More often than not, these two processes couple with each other so that separating them is practically challenging.

Serendipitously, our LES simulations (i.e., CTRL versus FXDLHF) are well suited for comparing the two. The reason is that inversion properties are similar between the two experiments whereas the boundary layer regimes during dissipation are dramatically different: Cu-coupled STBL in CTRL versus well-mixed STBL in FXDLHF. This constitutes a control experiment as the mechanism of CuPE operates in CTRL, but not in FXDLHF that is absent of Cu convection. The difference can be clearly seen in Fig. 9 showing the profiles of vertical velocity skewness during the breakup stages. We know that the sign of vertical velocity skewness reflects the driver of buoyancy (Moeng and Rotunno 1990), with positive and negative values suggesting bottom-heating driven and top-cooling driven, respectively. In the CTRL, the vertical velocity variance is typical of a Cu-coupled STBL in which the cloud-top radiative cooling and surface heating jointly drive the convection, leading to a mixture of positive and negative skewness (Fig. 9a). In contrast, convection in FXDLHF is primarily driven by cooling from above, as manifested by negatively skewed vertical velocities throughout most of the boundary layer except close to the inversion.

Figure 10 shows the cloud fraction versus κ. Both simulations show that cloud fraction decreases with κ, generally consistent with the CTEI theory, but their relationships differ in two respects. First, the change of cloud fraction with κ is more rapid in FXDLHF than in CTRL. The rapid dissipation eventually leads to a clear boundary layer, which behaves like a quick runaway process. This is consistent with the CTEI theory that predicts an unstable process driven by positive feedback. In contrast, the cloud fraction in CTRL gradually evolves from the Sc regime with full coverage to the Cu regime with a cloud cover of ~20%, consistent with the CuPE.

Second, Sc breaks up at a smaller κ in the CTRL than in FXDLHF. This appears to be a manifestation of the additional
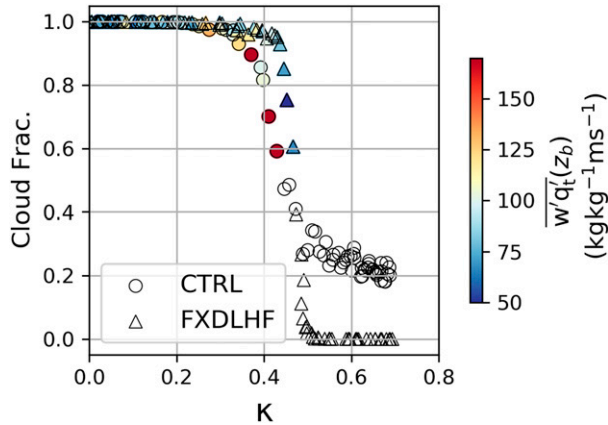
FIG. 10. Cloud fraction vs κ for CTRL and FXDLHF runs. Symbols are color-coded by the q_t flux at Sc cloud base (only those with cloud fraction greater than 0.5).
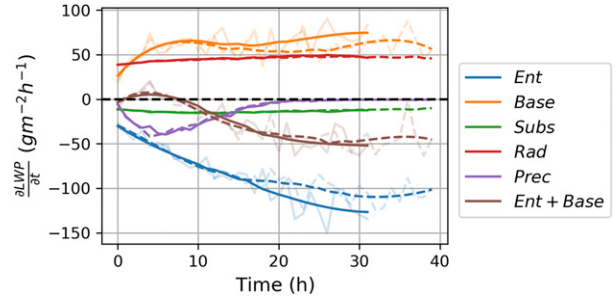

FIG. 11. Temporal evolutions of all forcing terms of LWP prognostic equation for CTRL (solid) and FXDLHF (dashed) runs. Plotted are clouds with cloudiness greater than 99%. Lines for Ent_{LWP} and $Base_{LWP}$ are after smoothing, and the unsmoothed values are marked by the semitransparent lines.

drying effect of the CuPE mechanism that only operates in CTRL run (CTEI should operate in both). This enhanced drying by CuPE is supported by the larger q_t flux at the cloud base in CTRL. According to Van der Dussen et al. (2014), CTEI predicts that larger cloud-base moisture flux enables the Sc deck to be sustained at a larger κ because of the more moisture supply compensating for the CTEI-induced desiccation. This argument from the CTEI-based reasoning is not supported by our simulations: Sc breaks up at a smaller κ when the cloud-base q_t flux is large. Such a result is more consistent with the CuPE theory predicting that dissipation is accompanied by stronger q_t flux at Sc base.

The above analysis confirms the role of Cu convection in breaking up the Sc deck. By not allowing the LHF to increase, Cu convection cannot develop so that the mechanism of CuPE is absent, leaving only the CETI mechanism to operate. This can postpone the dissipation of Sc deck, but, once the CETI initiates, a runaway effect dominates, shifting a well-mixed STBL to a clear boundary layer.

To further confirm the CuPE-induced drying, we use the budget analysis of LWP (Van der Dussen et al. 2013). Figure 11 shows the temporal evolutions of all the forcing terms of LWP tendency in CTRL (solid) and FXDLHF (dashed) runs. In the CTRL run, the stronger LHF leads to more moisture supply to the cloud layer, as shown by the $Base_{LWP}$ term. However, the larger LHF also strengthens the entrainment drying (Ent_{LWP}), desiccating the clouds. The entrainment drying starts to outweigh the moistening effect after $t = 20$ h as the Cu convection develops. Throughout the simulations, the combined effects of the changes in $Base_{LWP}$ and Ent_{LWP} due to the larger LHF is to dry the clouds, as shown by the more negative Ent_{LWP} + $Base_{LWP}$ for the CTRL run (brown lines). This finding supports the role of LHF in invigorating the Cu convection, promoting the breakup of the Sc deck.

Until now, we have addressed all the questions posed in section 3. The answers are summarized as follows:

Why does decoupling still happen even if the LHF is not allowed to increase?

The weak capping temperature inversion causes large entrainment efficiency that decouples the boundary layer.

Why does the boundary layer recouple after initial decoupling in the FXDLHF?

Without an increasing LHF, the high entrainment rate cannot be sustained because of the strengthening capping inversion. In addition, diabatic cooling of the cloud-layer increases, counteracting the entrainment warming.

Can the FXDLHF results be explained by the theoretical framework of BW97?

Yes.

Why is the Sc sustained longer in the FXDLHF even though the surface moisture supply is weaker?

There is no cumulus coupling during the dissipation phase of FXDLHF. This reduces the entrainment drying by cumulus penetration into the dry capping inversion. Such a cloud-favoring mechanism outweighs the cloud-reducing mechanism (i.e., reduced moisture supply from the surface).

How can the Sc dissipations in both runs be explained with existing theories such as the CTEI and the CuPE?

The CTEI explains well the Sc dissipation in the FXDLHF that is lack of cumulus penetration. In the CTRL, both mechanisms contribute. It is the CuPE mechanism that fastens the Sc dissipation in the CTRL relative to that in the FXDLHF.

6. Discussion

We have confirmed the indispensable role of LHF in driving the cloud transition during the ASTEX field campaign (Fig. 2), and have answered the questions posed in section 3. Here we discuss two key insights.

a. The importance of entrainment efficiency

The entrainment efficiency is crucially important for the LHF-driven cloud transitions, both as external forcing and as feedback. For the ASTEX case, the initial temperature jump across the capping inversion is weak enough ($\sim$5.5 K) to cause highly effective entrainment warming, which is the dominant

mechanism responsible for the boundary layer decoupling. As the deepening boundary layer erodes into a drier and less stable free atmosphere, evaporative cooling enhances, further increasing the entrainment efficiency. This acts to amplify the preexisting decoupling.

This partially explains the lack of a clear signal of the dependence of boundary layer decoupling on the LHF in observations. We know that the inversion strength of marine boundary layers presents considerable temporal and regional variations (Muhlbauer et al. 2014). The time scale of the lower-tropospheric stability (a proxy for the temperature inversion strength) variation is on the order of ~2 days (Eastman et al. 2016), comparable to the time scale of the cloud transition. The inversion strength variations can lead to variations in the entrainment efficiency (Caldwell et al. 2005; Wood 2012), altering the STBL coupling state to the extent that the signals of LHF are substantially diminished.

b. The physical meaning of Ent + Diab

We found Ent + Diab is a model diagnostic useful for a physical conceptualization of the boundary layer decoupling. The physical meaning of this diagnostic can be understood from two perspectives. From the perspective of cloud-layer energy balance, radiative cooling tends to balance the warming by entrainment and precipitation. An imbalance toward net warming (i.e., a more positive Ent + Diab) will cause a downward energy flux at the cloud base, a cooling effect to balance the excessive warming. Such a downward flux of energy near the cloud base is a manifestation of boundary layer decoupling (Bretherton 1997; Stevens 2000). Therefore, a larger Ent + Diab predicts a more decoupled boundary layer.

Another perspective is the idea of TKE budget. The Ent + Diab dictates the net generation of TKE: the radiative cooling produces the TKE while the entrainment and precipitation consume it. By neglecting the shear generation, the time evolution of the column-integrated TKE, $\widehat{TKE}$, can be approximated as

$$\frac{\partial \widehat{TKE}}{\partial t} \approx B - \varepsilon(\widehat{TKE}), \qquad (7)$$

where B measures the net buoyant generation of $\widehat{TKE}$ and ε is the viscous dissipation that is larger for higher $\widehat{TKE}$. The tendency term on the left is typically a magnitude smaller, leaving a rough balance between the two forcing terms: $B \approx \varepsilon(\widehat{TKE})$. A smaller Ent + Diab should correspond to a larger B and, therefore, a greater rate of TKE loss to small-scale viscous dissipation, meaning a more intense turbulent mixing.

Reconciling these two perspectives (cloud-layer energy budget versus boundary layer TKE budget) is straightforward. All the three processes dictated by Ent + Diab (entrainment, cloud-top radiative cooling, and precipitation) happens in the Sc deck that situates near the top of the boundary layer. Thus, the net warming of the Sc layer inevitably suppresses the generation of TKE, stabilizing the boundary layer.

This diagnostic, however, should not work for decoupling of an STBL drifting over colder water (Zheng and Li 2019). From the perspective of cloud-layer energy balance, cooling of the

underlying surface requires energy supply from above, which must cause downward energy flux somewhere in the boundary layer, leading to the decoupling. From the perspective of buoyancy budgets, the stabilization of the warm-advection flow suppresses the TKE, promoting the decoupling. Thus, an additional term that accounts for the strength of the temperature advection should be added to the Ent + Diab in order to generalize its usage to broader circumstances such as the middle latitudes.

7. Conclusions

Surface latent heat flux (LHF) has long been regarded as a crucial controller of stratocumulus (Sc)-to-cumulus (Cu) transition (Krueger et al. 1995; BW97; Wyant et al. 1997). A necessary condition for the cloud transition is sea surface warming. As seawater warms up, the LHF must increase, constrained by the Clausius–Clapeyron physics and boundary layer conservation laws. Such an increase in LHF has been argued to drive the two stages of the Sc-to-Cu transition, namely, the boundary layer decoupling (first stage) and the breakup of the Sc deck (second stage). This idea, however, is challenged by recent field observations showing no distinct dependence of the boundary layer coupling state on the LHF (Jones et al. 2011; Zhou et al. 2015). Given the mixed lines of evidence, it is imperative to further investigate the underlying mechanism of LHF influences on cloud transitions.

This study uses LES to isolate the role of increased LHF by conducting a mechanism-denial experiment (FXDLHF) that turns off the LHF adjustment, that is, the LHF is not permitted to increase with the warming sea surface. By comparing it with the control run for a classical Sc-to-Cu transition case from the ASTEX field campaign (CTRL), we can identify how the increase in LHF influences the cloud transitions. The LES modeling results are interpreted in the theoretical frameworks of cloud-layer energy and water balances and a mixed-layer model (BW97). The results are summarized as follows:

- The increase in LHF is not a necessary condition for the initiation of boundary layer decoupling. For the ASTEX case, the initial temperature jump across the capping inversion is weak enough (~5.5 K) to cause highly effective entrainment warming, which dominantly drives the decoupling. Such a large influence of the entrainment efficiency might explain the lack of observational evidence for the LHF control on the boundary layer decoupling, given the marked variations of the inversion strength (thereby entrainment efficiency) in time and space.

- The decoupling due to the weak inversion alone, however, cannot be sustained without the help of the LHF adjustment. Without an increase of LHF with SST, the boundary layer tends to dry more rapidly due to entrainment, elevating the lifting condensation level (LCL). The growing LCL eventually intercepts with the Sc deck base, recoupling the boundary layer. Energetically speaking, without an increase in LHF to sustain a strong entrainment rate, the entrainment warming can no longer combat the increased diabatic cooling (e.g., increased radiative cooling) as the boundary layer deepens. This ultimately recouples the boundary layer. This result confirms the indispensable role of LHF adjustment in sustaining (although not initiating) the boundary layer decoupling.
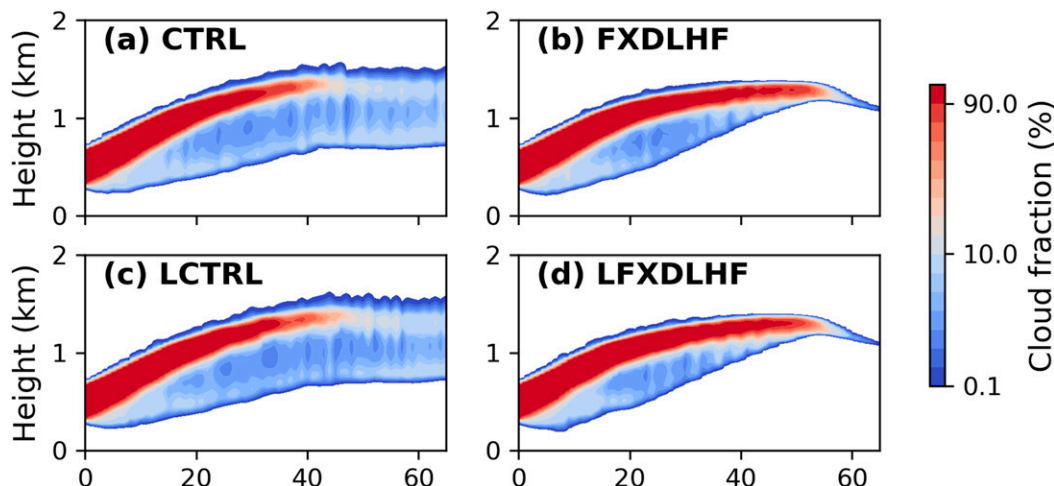
FIG. A1. Time–height plots of cloud fraction for the simulations of (a) CTRL, (b) FXDLHF, (c) LCTRL, and (d) LFXDLHF.

- The absence of LHF adjustment tends to delay the breakup of the Sc deck. Without the LHF increase, the Cu convection cannot develop so that the enhanced entrainment drying due to the Cu penetration into the dry inversion cannot happen. This helps to sustain the Sc deck longer by ~10 h, even though the surface moisture supply is lower. For the same reason, the transition to Cu regime can never happen without LHF adjustment. This result confirms the theory of "Cu penetrative entrainment" proposed by Wyant et al. (1997).

Last, this study finds a model diagnostic that is useful for a physical conceptualization of the boundary layer decoupling: Ent + Diab, in which the Ent is the entrainment warming and the Diab is the diabatic cooling (a combination of radiative cooling and precipitation-induced warming) across the cloud layer, both having the unit of watts per square meter. This diagnostic can help organize our observational and modeling analyses of Sc-to-Cu transitions.

APPENDIX

Simulations in a Larger Domain

To examine the sensitivity of the results to the domain size, we run the same set of experiments over a larger domain with the size of 8960 m × 8960 m, denoted as LCTRL and LFXDLHF. Comparing these two sets of experiments (i.e., 4480 m × 4480 m vs 8960 m × 8960 m) shows almost no influence of the domain size on the results (Fig. A1).

REFERENCES

Abel, S. J., and Coauthors, 2017: The role of precipitation in controlling the transition from stratocumulus to cumulus clouds in a Northern Hemisphere cold-air outbreak. *J. Atmos. Sci.*, **74**, 2293–2314, https://doi.org/10.1175/JAS-D-16-0362.1.

Albrecht, B. A., C. S. Bretherton, D. Johnson, W. H. Schubert, and A. S. Frisch, 1995: The Atlantic Stratocumulus Transition Experiment—ASTEX. *Bull. Amer. Meteor. Soc.*, **76**, 889–904, https://doi.org/10.1175/1520-0477(1995)076<0889:TASTE>2.0.CO;2.

Bodas-Salcedo, A., and Coauthors, 2014: Origins of the solar radiation biases over the Southern Ocean in CFMIP2 models. *J. Climate*, **27**, 41–56, https://doi.org/10.1175/JCLI-D-13-00169.1.

Bretherton, C. S., 1997: Convection in stratocumulus-topped atmospheric boundary layers. *The Physics and Parameterization of Moist Atmospheric Convection*, Springer, 127–142.

——, and M. C. Wyant, 1997: Moisture transport, lower-tropospheric stability, and decoupling of cloud-topped boundary layers. *J. Atmos. Sci.*, **54**, 148–167, https://doi.org/10.1175/1520-0469(1997)054<0148:MTLTSA>2.0.CO;2.

——, and P. N. Blossey, 2014: Low cloud reduction in a greenhouse-warmed climate: Results from Lagrangian LES of a subtropical marine cloudiness transition. *J. Adv. Model. Earth Syst.*, **6**, 91–114, https://doi.org/10.1002/2013MS000250.

——, ——, and J. Uchida, 2007: Cloud droplet sedimentation, entrainment efficiency, and subtropical stratocumulus albedo. *Geophys. Res. Lett.*, **34**, L03813, https://doi.org/10.1029/2006GL027648.

——, J. Uchida, and P. N. Blossey, 2010: Slow manifolds and multiple equilibria in stratocumulus-capped boundary layers. *J. Adv. Model. Earth Syst.*, **2** (4), https://doi.org/10.3894/JAMES.2010.2.14.

Caldwell, P., C. S. Bretherton, and R. Wood, 2005: Mixed-layer budget analysis of the diurnal cycle of entrainment in southeast Pacific stratocumulus. *J. Atmos. Sci.*, **62**, 3775–3791, https://doi.org/10.1175/JAS3561.1.

Deardorff, J., 1980: Cloud top entrainment instability. *J. Atmos. Sci.*, **37**, 131–147, https://doi.org/10.1175/1520-0469(1980)037<0131:CTEI>2.0.CO;2.

de Roode, S. R., and P. G. Duynkerke, 1997: Observed Lagrangian transition of stratocumulus into cumulus during ASTEX: Mean state and turbulence structure. *J. Atmos. Sci.*, **54**, 2157–2173, https://doi.org/10.1175/1520-0469(1997)054<2157:OLTOSI>2.0.CO;2.

Eastman, R., R. Wood, and C. S. Bretherton, 2016: Time scales of clouds and cloud-controlling variables in subtropical stratocumulus from a Lagrangian perspective. *J. Atmos. Sci.*, **73**, 3079–3091, https://doi.org/10.1175/JAS-D-16-0050.1.

Emanuel, K. A., 1994: *Atmospheric Convection.* Oxford University Press, 580 pp.

Geerts, B., 2019: Cold-Air Outbreaks in the Marine Boundary Layer Experiment (COMBLE) science implementation plan. ARM Tech. Rep. DOE/SC-ARM-19-002, 38 pp.

Hahn, C. J., and S. G. Warren, 2007: A gridded climatology of clouds over land (1971-96) and ocean (1954-97) from surface observations worldwide. Oak Ridge National Laboratory Carbon Dioxide Information Analysis Center Rep., 75 pp.

Hartmann, D. L., M. E. Ockert-Bell, and M. L. Michelsen, 1992: The effect of cloud type on Earth's energy balance: Global analysis. *J. Climate*, **5**, 1281–1304, https://doi.org/10.1175/1520-0442(1992)005<1281:TEOCTO>2.0.CO;2.

Iacono, M. J., J. S. Delamere, E. J. Mlawer, M. W. Shephard, S. A. Clough, and W. D. Collins, 2008: Radiative forcing by long-lived greenhouse gases: Calculations with the AER radiative transfer models. *J. Geophys. Res.*, **113**, D13103, https://doi.org/10.1029/2008JD009944.

Jones, C., C. Bretherton, and D. Leon, 2011: Coupled vs. decoupled boundary layers in VOCALS-REx. *Atmos. Chem. Phys.*, **11**, 7143–7153, https://doi.org/10.5194/acp-11-7143-2011.

Kazemirad, M., and M. A. Miller, 2020: Summertime post-cold-frontal marine stratocumulus transition processes over the eastern North Atlantic. *J. Atmos. Sci.*, **77**, 2011–2037, https://doi.org/10.1175/JAS-D-19-0167.1.

Khairoutdinov, M., and Y. Kogan, 2000: A new cloud physics parameterization in a large-eddy simulation model of marine stratocumulus. *Mon. Wea. Rev.*, **128**, 229–243, https://doi.org/10.1175/1520-0493(2000)128<0229:ANCPPI>2.0.CO;2.

——, and D. A. Randall, 2003: Cloud resolving modeling of the ARM summer 1997 IOP: Model formulation, results, uncertainties, and sensitivities. *J. Atmos. Sci.*, **60**, 607–625, https://doi.org/10.1175/1520-0469(2003)060<0607:CRMOTA>2.0.CO;2.

Klein, S. A., D. L. Hartmann, and J. R. Norris, 1995: On the relationships among low-cloud structure, sea surface temperature, and atmospheric circulation in the summertime northeast Pacific. *J. Climate*, **8**, 1140–1155, https://doi.org/10.1175/1520-0442(1995)008<1140:OTRALC>2.0.CO;2.

Krueger, S. K., G. T. McLean, and Q. Fu, 1995: Numerical simulation of the stratus-to-cumulus transition in the subtropical marine boundary layer. Part II: Boundary-layer circulation. *J. Atmos. Sci.*, **52**, 2851–2868, https://doi.org/10.1175/1520-0469(1995)052<2851:NSOTST>2.0.CO;2.

Kuo, H. C., and W. H. Schubert, 1988: Stability of cloud-topped boundary layers. *Quart. J. Roy. Meteor. Soc.*, **114**, 887–916, https://doi.org/10.1002/qj.49711448204.

Lewellen, D., and W. Lewellen, 1998: Large-eddy boundary layer entrainment. *J. Atmos. Sci.*, **55**, 2645–2665, https://doi.org/10.1175/1520-0469(1998)055<2645:LEBLE>2.0.CO;2.

Lilly, D. K., 1968: Models of cloud-topped mixed layers under a strong inversion. *Quart. J. Roy. Meteor. Soc.*, **94**, 292–309, https://doi.org/10.1002/qj.49709440106.

Lloyd, G., and Coauthors, 2018: In situ measurements of cloud microphysical and aerosol properties during the break-up of stratocumulus cloud layers in cold air outbreaks over the North Atlantic. *Atmos. Chem. Phys.*, **18**, 17 191–17 206, https://doi.org/10.5194/acp-18-17191-2018.

Lock, A., 2009: Factors influencing cloud area at the capping inversion for shallow cumulus clouds. *Quart. J. Roy. Meteor. Soc.*, **135**, 941–952, https://doi.org/10.1002/qj.424.

McCoy, I. L., R. Wood, and J. K. Fletcher, 2017: Identifying meteorological controls on open and closed mesoscale cellular convection associated with marine cold air outbreaks. *J. Geophys. Res. Atmos.*, **122**, 11 678–11 702, https://doi.org/10.1002/2017JD027031.

Moeng, C.-H., and R. Rotunno, 1990: Vertical-velocity skewness in the buoyancy-driven boundary layer. *J. Atmos. Sci.*, **47**, 1149–1162, https://doi.org/10.1175/1520-0469(1990)047<1149:VVSITB>2.0.CO;2.

Muhlbauer, A., I. L. McCoy, and R. Wood, 2014: Climatology of stratocumulus cloud morphologies: Microphysical properties and radiative effects. *Atmos. Chem. Phys.*, **14**, 6695–6716, https://doi.org/10.5194/acp-14-6695-2014.

Neggers, R., and Coauthors, 2017: Single-column model simulations of subtropical marine boundary-layer cloud transitions under weakening inversions. *J. Adv. Model. Earth Syst.*, **9**, 2385–2412, https://doi.org/10.1002/2017MS001064.

Nicholls, S., 1984: The dynamics of stratocumulus: Aircraft observations and comparisons with a mixed layer model. *Quart. J. Roy. Meteor. Soc.*, **110**, 783–820, https://doi.org/10.1002/qj.49711046603.

——, and J. Leighton, 1986: An observational study of the structure of stratiform cloud sheets: Part I. Structure. *Quart. J. Roy. Meteor. Soc.*, **112**, 431–460, https://doi.org/10.1002/qj.49711247209.

——, and J. Turton, 1986: An observational study of the structure of stratiform cloud sheets: Part II. Entrainment. *Quart. J. Roy. Meteor. Soc.*, **112**, 461–480, https://doi.org/10.1002/qj.49711247210.

Randall, D. A., 1980: Conditional instability of the first kind upside-down. *J. Atmos. Sci.*, **37**, 125–130, https://doi.org/10.1175/1520-0469(1980)037<0125:CIOTFK>2.0.CO;2.

Riehl, H., T. Yeh, J. S. Malkus, and N. E. La Seur, 1951: The northeast trade of the Pacific Ocean. *Quart. J. Roy. Meteor. Soc.*, **77**, 598–626, https://doi.org/10.1002/qj.49707733405.

Romps, D. M., 2017: Exact expression for the lifting condensation level. *J. Atmos. Sci.*, **74**, 3891–3900, https://doi.org/10.1175/JAS-D-17-0102.1.

Sandu, I., and B. Stevens, 2011: On the factors modulating the stratocumulus to cumulus transitions. *J. Atmos. Sci.*, **68**, 1865–1881, https://doi.org/10.1175/2011JAS3614.1.

Siems, S. T., and C. S. Bretherton, 1992: A numerical investigation of cloud-top entrainment instability and related experiments. *Quart. J. Roy. Meteor. Soc.*, **118**, 787–818, https://doi.org/10.1002/qj.49711850702.

——, ——, M. B. Baker, S. Shy, and R. E. Breidenthal, 1990: Buoyancy reversal and cloud-top entrainment instability. *Quart. J. Roy. Meteor. Soc.*, **116**, 705–739, https://doi.org/10.1002/qj.49711649309.

Smolarkiewicz, P. K., and W. W. Grabowski, 1990: The multidimensional positive definite advection transport algorithm: Nonoscillatory option. *J. Comput. Phys.*, **86**, 355–375, https://doi.org/10.1016/0021-9991(90)90105-A.

Stevens, B., 2000: Cloud transitions and decoupling in shear-free stratocumulus-topped boundary layers. *Geophys. Res. Lett.*, **27**, 2557–2560, https://doi.org/10.1029/1999GL011257.

——, 2002: Entrainment in stratocumulus-topped mixed layers. *Quart. J. Roy. Meteor. Soc.*, **128**, 2663–2690, https://doi.org/10.1256/qj.01.202.

——, 2007: On the growth of layers of nonprecipitating cumulus convection. *J. Atmos. Sci.*, **64**, 2916–2931, https://doi.org/10.1175/JAS3983.1.

——, and Coauthors, 2003: Dynamics and Chemistry of Marine Stratocumulus—DYCOMS-II. *Bull. Amer. Meteor. Soc.*, **84**, 579–594, https://doi.org/10.1175/BAMS-84-5-579.

Teixeira, J., and Coauthors, 2011: Tropical and subtropical cloud transitions in weather and climate prediction models: The GCSS/WGNE Pacific Cross-Section Intercomparison (GPCI). *J. Climate*, **24**, 5223–5256, https://doi.org/10.1175/2011JCLI3672.1.

Turton, J. D., and S. Nicholls, 1987: A study of the diurnal variation of stratocumulus using a multiple mixed layer model. *Quart. J. Roy. Meteor. Soc.*, **113**, 969–1009, https://doi.org/10.1002/qj.49711347712.

Van der Dussen, J., and Coauthors, 2013: The GASS/EUCLIPSE model intercomparison of the stratocumulus transition as observed during ASTEX: LES results. *J. Adv. Model. Earth Syst.*, **5**, 483–499, https://doi.org/10.1002/jame.20033.

——, S. De Roode, and A. Siebesma, 2014: Factors controlling rapid stratocumulus cloud thinning. *J. Atmos. Sci.*, **71**, 655–664, https://doi.org/10.1175/JAS-D-13-0114.1.

Wood, R., 2012: Stratocumulus clouds. *Mon. Wea. Rev.*, **140**, 2373–2423, https://doi.org/10.1175/MWR-D-11-00121.1.

——, and C. S. Bretherton, 2006: On the relationship between stratiform low cloud cover and lower-tropospheric stability. *J. Climate*, **19**, 6425–6432, https://doi.org/10.1175/JCLI3988.1.

Wyant, M. C., C. S. Bretherton, H. A. Rand, and D. E. Stevens, 1997: Numerical simulations and a conceptual model of the stratocumulus to trade cumulus transition. *J. Atmos. Sci.*, **54**, 168–192, https://doi.org/10.1175/1520-0469(1997)054<0168:NSAACM>2.0.CO;2.

Xiao, H., C.-M. Wu, and C. R. Mechoso, 2011: Buoyancy reversal, decoupling and the transition from stratocumulus to shallow cumulus topped marine boundary layers. *Climate Dyn.*, **37**, 971–984, https://doi.org/10.1007/s00382-010-0882-3.

Yamaguchi, T., and D. A. Randall, 2008: Large-eddy simulation of evaporatively driven entrainment in cloud-topped mixed layers. *J. Atmos. Sci.*, **65**, 1481–1504, https://doi.org/10.1175/2007JAS2438.1.

Zheng, Y., and Z. Li, 2019: Episodes of warm-air advection causing cloud-surface decoupling during the MARCUS. *J. Geophys. Res. Atmos.*, **124**, 12 227–12 243, https://doi.org/10.1029/2019JD030835.

——, D. Rosenfeld, and Z. Li, 2018: Estimating the decoupling degree of subtropical marine stratocumulus decks from satellite. *Geophys. Res. Lett.*, **45**, 12 560–12 568, https://doi.org/10.1029/2018GL078382.

——, ——, and ——, 2020: A more general paradigm for understanding the decoupling of stratocumulus-topped boundary layers: The importance of horizontal temperature advection. *Geophys. Res. Lett.*, **47**, e2020GL087697, https://doi.org/10.1029/2020GL087697.

Zhou, X., P. Kollias, and E. R. Lewis, 2015: Clouds, precipitation, and marine boundary layer structure during the MAGIC field campaign. *J. Climate*, **28**, 2420–2442, https://doi.org/10.1175/JCLI-D-14-00320.1.